



Article

Machine Learning Approach for Prediction and Reliability Analysis of Failure Strength of U-Shaped Concrete Samples Joined with UHPC and PUC Composites

Sadi I. Haruna ^{1,2,*}, Yasser E. Ibrahim ^{1,*}  and Ibrahim Khalil Umar ³

¹ Engineering Management Department, College of Engineering, Prince Sultan University, Riyadh 11586, Saudi Arabia

² School of Civil Engineering, Tianjin University, Tianjin 300350, China

³ Department of Civil Engineering Technology, Kano State Polytechnic, Kano 700282, Nigeria; ikumar@kanopoly.edu.ng

* Correspondence: sharuna@psu.edu.sa (S.I.H.); ymansour@psu.edu.sa (Y.E.I.)

Abstract: To meet the increasing demand for resilient infrastructure in seismic and high-impact areas, accurate prediction and reliability analysis of the performance of composite structures under impact loads is essential. Conventional techniques, including experimental testing and high-quality finite element simulation, require considerable time and resources. To address these issues, this study investigated individual and hybrid models including support vector regression (SVR), Gaussian process regression (GPR), and improved eliminate particle swarm optimization hybridized artificial neural network (IEPANN) models for predicting the failure strength of composite concrete developed by combining normal concrete (NC) with ultra-high performance concrete (UHPC) and polyurethane-based polymer concrete (PUC), considering different surface treatments and subjected to various static and impact loads. An experimental dataset was utilized to train the ML models and perform the reliability analysis on the impact dataset. Key parameters included compressive strength (C_{fc}), flexural load of the U-shaped specimens (P), density (ρ), first crack strength (N_1), and splitting tensile strength (f_t). Results revealed that all the developed models had high prediction accuracy, achieving NSE values above acceptable thresholds greater than 90% across all the datasets. Statistical errors such as RMSE, MAE, and PBIAS were calculated to fall within acceptable limits. Hybrid IEPANN appeared to be the most effective model, demonstrating the highest NSE value of 0.999 and the lowest RMSE, PBIAS, and MAE values of 0.0013, 0.0018, and 0.001, respectively. The reliability analysis revealed that impact times (N_1 and N_2) reduced as the survival probability increased.



Academic Editor: Peng Zhang

Received: 5 December 2024

Revised: 18 December 2024

Accepted: 3 January 2025

Published: 6 January 2025

Citation: Haruna, S.I.; Ibrahim, Y.E.; Umar, I.K. Machine Learning Approach for Prediction and Reliability Analysis of Failure Strength of U-Shaped Concrete Samples Joined with UHPC and PUC Composites. *J. Compos. Sci.* **2025**, *9*, 23. <https://doi.org/10.3390/jcs9010023>

Copyright: © 2025 by the authors. Licensee MDPI, Basel, Switzerland. This article is an open access article distributed under the terms and conditions of the Creative Commons Attribution (CC BY) license (<https://creativecommons.org/licenses/by/4.0/>).

Keywords: composite concrete; machine learning; reliability analysis; impact load; UHPC

1. Introduction

Concrete structures experience a variety of structural and durability concerns during their serviceability [1,2]. For instance, bridge columns are eroded by seawater, heat stress or impact loads can damage railway base joints, and concrete elements can be damaged by falling objects. Therefore, effective repair is required to prolong their service life [1,3]. During concrete restoration, the interface between the concrete and repair materials is weak [4]. The interfacial strength primarily depends entirely on the concrete being properly repaired. The impairment of the repair materials is attributed to two factors: firstly,

chemical bonding at the composite interface (old concrete and the repair materials) [5]; and second, interfacial friction in the composite [5], which depends on the first factor. The bond capacity between the old and new materials has the most influence on the first phase, while the repair material's effectiveness has the greatest impact on the second [5]. As a result, effective repair requires appropriate repair materials as well as adequate bonding qualities at the repair interface. Widely used repair and retrofitting approaches include steel and concrete jackets [6,7], fiber-reinforced polymer confinement [8,9], and PU grouting substances [10,11]. However, some techniques are difficult to implement and costly.

The impact properties of plain and steel-fiber-reinforced concrete (SFRC) subjected to repeated drop-weight impact have previously been statistically evaluated [12]. Song et al. [13] studied the synergic influence of steel and steel-polypropylene fibers on the impact resistance and performed reliability analysis of FRC using a drop-weight impact testing method. Alavi et al. [14] compared the drop-weight impact results of plain concrete and FRC specimens with finite element analysis based on an ACI committee 544 testing procedure. The authors reported that both the numerical and experimental results revealed that impact resistance of the concrete specimens increased with increases in fiber volume fraction. AlAhmed et al. [15] evaluated the properties of sandwich panels through investigating different design features and main geometries. Using FE and regression analysis performed on 27 numerical experiments, the results indicated that a tubular sandwich element demonstrated least deformation and minimal destruction while influencing the maximum kinetic energy propagation. Recently, Al-shawafi et al. [16] evaluated the impact strength of UHPC retrofitted with different polyurethane grouting material thickness under impact loads. The authors utilized the two-parameter Weibull distribution function to analyze the impact test results. The results indicated that the polyurethane grouting material cast U-shaped UHPC had remarkably enhanced impact strength, which increased with increases in the thickness of the overlaid polyurethane grouting. Su et al. [17] developed extensive Karagozian & Case Concrete (KCC) and a reliable parameter generation method for estimating the impact properties of UHPC elements under impact loads. The authors comprehensively calibrated the failure surface, damage evolution, and other important parameters from the available experimental and analytical data for UHPC. Generally, the statistical technique is most commonly used method for investigating the impact strength of cement-based materials under multiple drop-weight impact testing, as found in the literature [12–14,18–20].

However, numerous research studies have been undertaken utilizing machine learning models to solve engineering problems, proving promising. Particular models have been applied in certain situations, but, no superior model has been reported to suit all cases [21–27]. As a result, adopting ensemble methods produces more accurate predictions. Yazici et al. [28] developed a radial basis function network (RBFN) model for predicting the impact strength of concrete incorporated with basalt, limestone, and natural aggregate as the main aggregate materials and subjected the concrete specimens to repeated drop-weight impact testing. The results indicated that the RBFN model was effective in predicting the impact strength of the concrete. Moein et al. [29] used the Weibull distribution function to perform reliability analysis on the impact test results of concrete incorporated with poly-olefin fiber under multiple impact loads. The result revealed that the Weibull distribution function successfully predicted the impact failure strength of the concrete. Mane et al. [30] developed an ANN model for estimating the impact resistance of concrete that included industrial waste and artificial sand; the ANN model provided high prediction accuracy. Another study [31] reported some limitations of linear regression models in predicting the shear modulus and damping coefficient of polymer concrete when associated with shear deformation of no more than $10^{-2}\%$. Li et al. [32] developed a deep neural network (DNN)

to predict the mechanical properties of polymer concrete panels. The results showed that neural networks with fewer neurons in a layer demonstrated lower convergence rates than neural networks with high numbers of neurons in a layer. Conversely, the IEPANN model is trained according to initial weight and bias, and the MSE between the experimental and estimated values is then calculated. Optimization is carried out based on this method until the stopping requirements are met, and smaller MSE value or peak iterations can be the stopping criteria. The performance of the developed IEPANN relies mainly on the selection of neurons and hidden layers. Some studies [33,34] have recommended that one (1) hidden layer is efficient for various regression models.

Ensemble approaches have been used in many engineering fields [35–40]. Liang et al. [36] developed an interpretable ensemble ML technique to estimate concrete creep properties, which included random forest (RF), extreme (XGBoost), and light gradient boosting and (LGBM). The authors reported that the ensemble models demonstrate higher prediction accuracy compared with the equation established by the fib Model Code 2010. Zhang et al. [38] predicted the flexural capacity of reinforced concrete (RC) beam-wrapped fiber-reinforced polymer (FRP) using ensemble ML, namely, gradient boosting decision tree, RF, XGBoost, and adaptive boosting. The ensemble ML performance was compared with empirical models, and the results showed the significant superiority of the ensemble ML model. Similarly, the maximum bond behavior between UHPC and reinforcement was predicted by Farouk et al., using an ensemble ML model [41]. You et al. [42] established novel hybrid ML models to forecast the maximum bond capacity between UHPC and reinforcement. The results revealed that the embedded depth remarkably influenced the bond strength of UHPC. Kan et al. [43] developed a deep learning algorithm for discovering cracks on a railway sleeper using the U-Net model. The authors proposed an improved U-net architecture for sectioning the cracks. Anas et al. [20] estimated the behavior of concrete slabs wrapped with different fiber types under impact stress, utilizing a 3-D finite element (FE) model for the estimation. The results indicated that the strengthening approach improved the RC slab's impact strength with regard to displacement and damage severity. Cui et al. [44] developed a novel model for estimating the dynamic shear stress and ultimate deflection of beams under impact load. Bakhshi et al. [45] proposed logarithmic-scale models to forecast the failure properties of concrete containing different fibers under multiple impact stress. The novel model forecasted and determined the effect of steel fibers on the post-cracking performance of FRC. The proposed model improved the estimation of the measured results obtained from impact testing conducted in previous studies for a different volume of steel fiber. Similarly, the failure strength of concrete modified with polyurethane binder was predicted by Lagsum et al. [46], using SVR and ANN models. Through advanced ML models, it is feasible to incorporate variables that possibly affect the composite structures.

The main aim of this study was to accurately model and predict the failure strength of composite structures under multiple impact loads. Furthermore, reliability analysis through Weibull distribution was performed on the test results to evaluate the design impact strength and impact resistance of composite U-shaped specimens subjected to repeated impact loads. This study employed hybrid IEPANN with an ANN model to form an ensemble IEPANN for prediction of the failure strength of composite U-shaped concrete. The predictive performance of IEPANN was compared with classical regression models including GPR and SVR. This study contributes to the field by providing a deeper understanding of the impact behavior of composite concrete structures and advancing ML applications in predicting and explaining material performance, as this research involves both static and impact variables for estimating the failure strength of composite concrete. The research can reduce the need for high-cost experimental programs and save time.

2. Development of Database

The impact strength data was obtained through the U-shaped repeated impact test (USDWIT), a unique testing approach adopted to determine concrete impact strength [11,47–49]. The technique utilizes a U-shape sample to determine the concrete's impact behavior through multiple drop-weight impacts (see Figure 1). The dataset used for developing the ML algorithms and the reliability analysis was obtained from these experiments [50,51]. Five (5) variables were used as input parameters, including compressive strength (C_{fc}), flexural stress of the U-shaped specimen (P), the density (ρ), first crack strength ($N1$), and splitting tensile strength (f_t). The failure strength ($N2$) was computed as the output parameter.

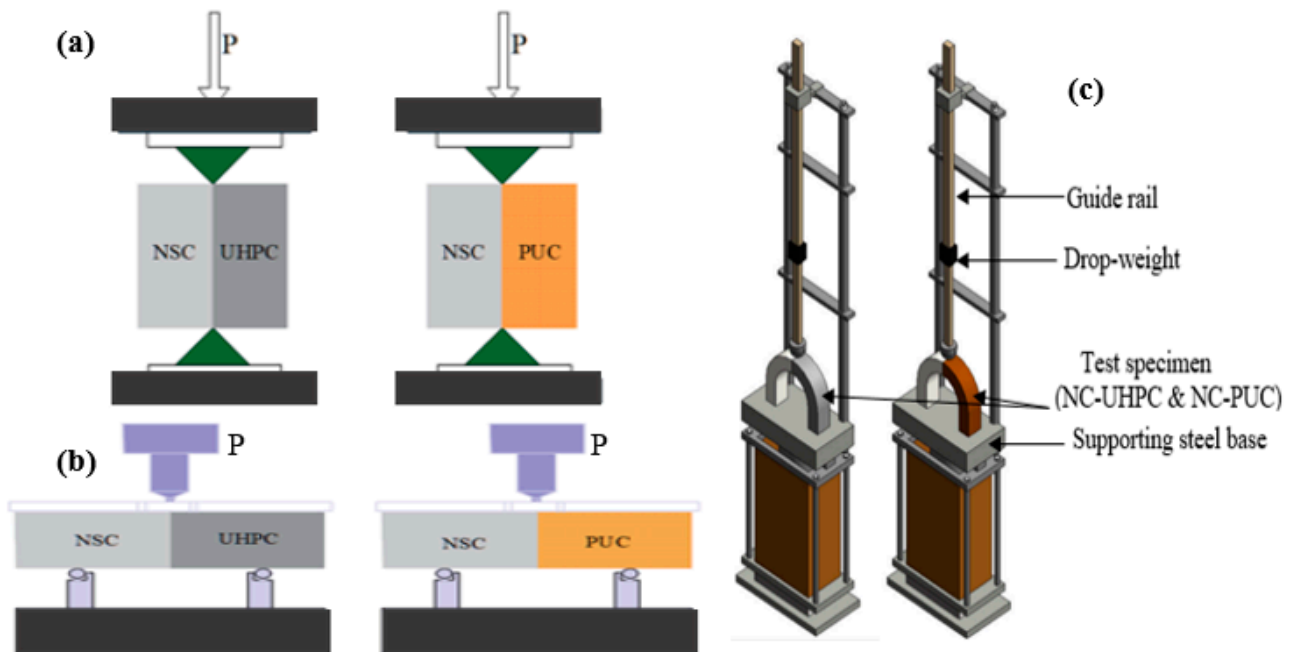


Figure 1. Experimental setup: (a) splitting tensile, (b) flexural, and (c) impact tests.

2.1. Description of Dataset Distribution

The data distribution was used to evaluate the datasets and characterize their nature, comprising six (6) variables obtained from the static and drop-weight impact testing. The variation and distribution plot of each input variable and output parameter is shown in Figure 2, showing that some of the input variables nearly followed normal distribution, including first crack strength ($N1$) and failure strength ($N2$), while input variable density (ρ) was normally distributed. On the other hand, parameters including splitting tensile (f_t) and compressive strength of the composite (C_{fc}), and flexural strength of the U-shaped specimen under static load barely followed normal distribution.

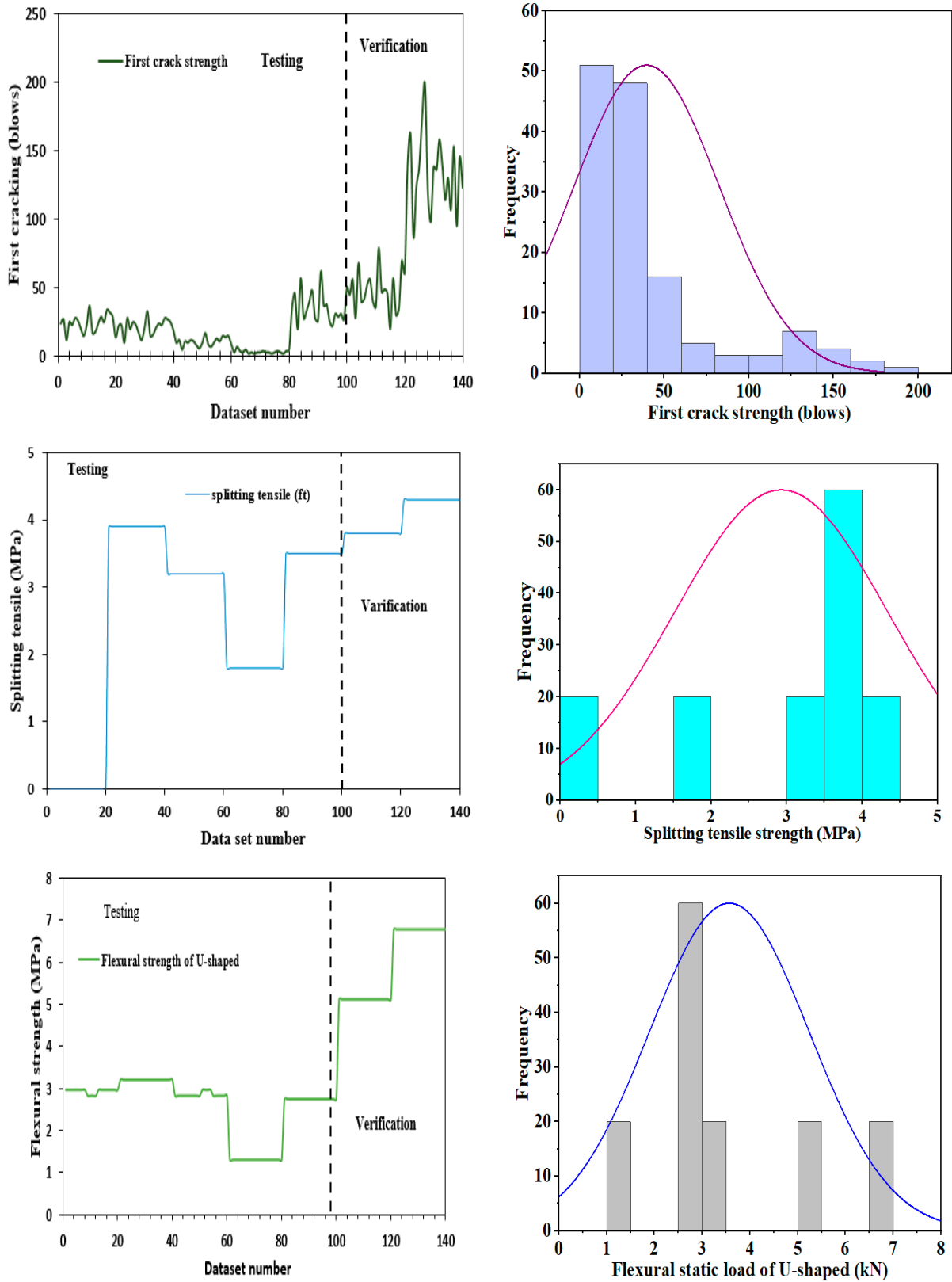


Figure 2. Cont.

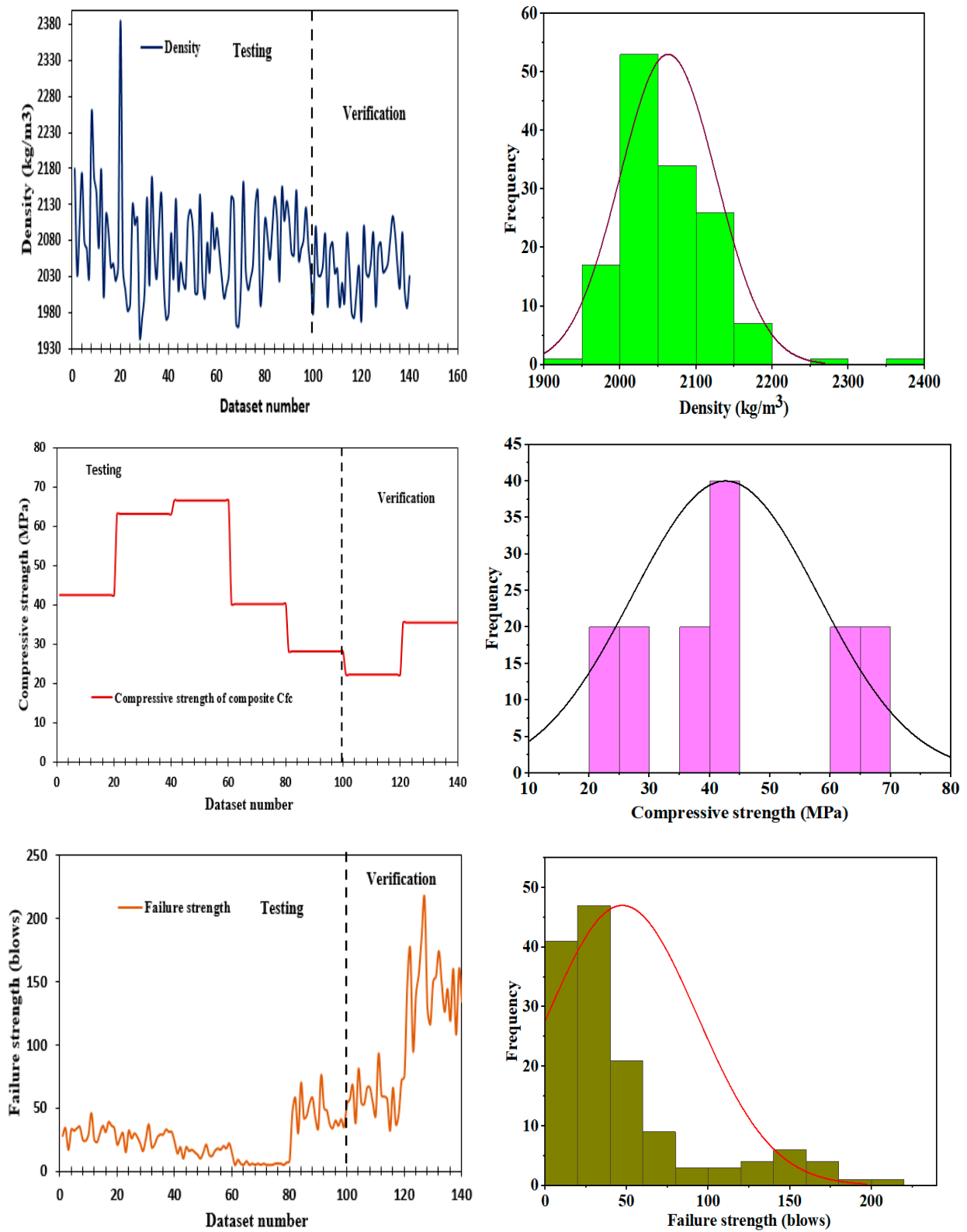


Figure 2. Variation of the datasets and distribution plot.

2.2. Selection of Optimal Input Variables

Table 1 shows the statistical analysis of the experimental dataset used for the modeling task. The analysis indicated the statistical parameters of the dataset to be suitable for developing an AI-based model. The selection of input variables when developing the model is essential for attaining the expected accurate prediction skills. As a result, introducing

unfitting factors in the modeling decreases the prediction accuracy [52]. However, insufficient input variables can result from low prediction skills. In this investigation, Pearson correlation was utilized to obtain the most relevant input features when evaluating the N_2 values of the composite U-shaped concrete samples. The Pearson correlation between the observed and predicted parameters is depicted in Figure 3. All the observed parameters exhibited reasonable correlation with the predicted parameter values. However, initial crack strength (N_1) showed the highest correlation with target parameter.

Table 1. Statistical parameters of the experimental data.

	f_t (MPa)	C_{fc} (MPa)	P (kN)	ρ (kg/m ³)	N_1 (Blow)	N_2 (Blow)
Min	0.00	22.30	1.31	1946.11	2.00	5.00
Max	4.30	66.50	6.78	2385.03	198.00	216.00
mean	2.93	42.61	3.57	2063.12	39.61	47.31
SD	1.41	15.49	1.68	63.20	42.93	45.95
Kurtosis	-0.02	-1.19	-0.42	3.95	2.42	2.12
Skewness	-1.15	0.41	0.75	1.21	1.78	1.68

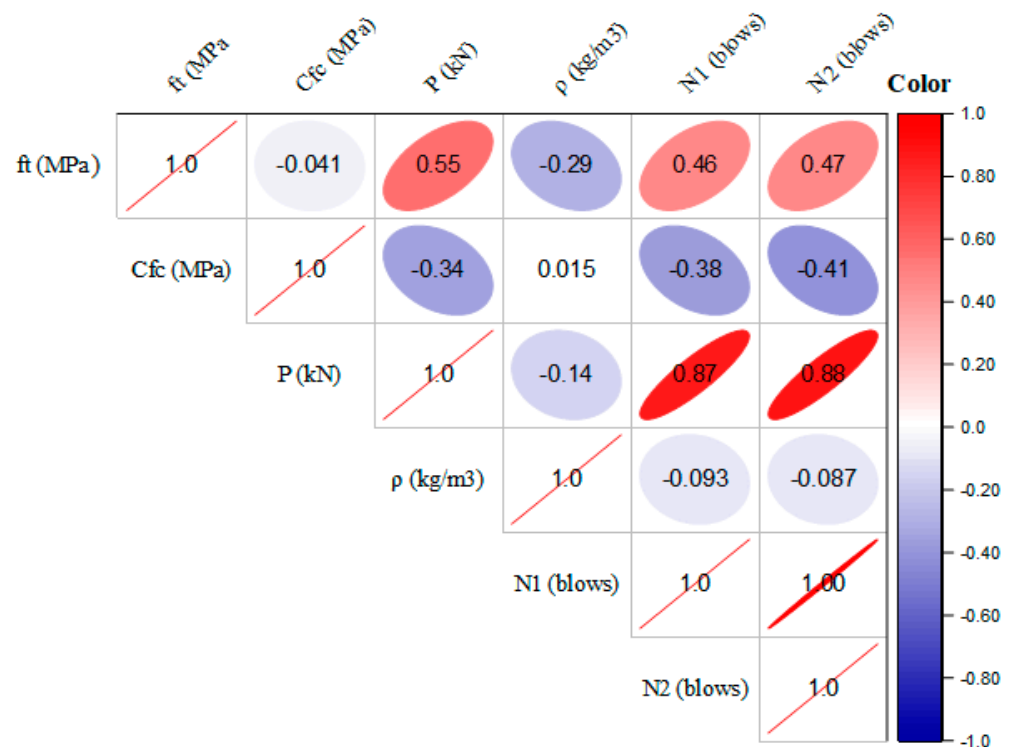


Figure 3. Correlation matrix between the input and output parameters.

3. Machine Learning Algorithm

3.1. Gaussian Process Regression (GPR)

GPR is a robust non-linear prediction model that improves the accuracy of aligning measured and predicted values of engineering properties [53]. The adoption of this model is substantiated by its efficiency in previous studies [53,54]. The GPR model was simulated using the exponential kernel function, which applied Bayesian inference of the dataset (Equation (1)), where x_i and y_i are input and output parameters, respectively). The GPR architecture is shown in Figure 4.

$$Q = \{(x_i, y_i), i = 1, 2, 3, 4, \dots, N\} \tag{1}$$

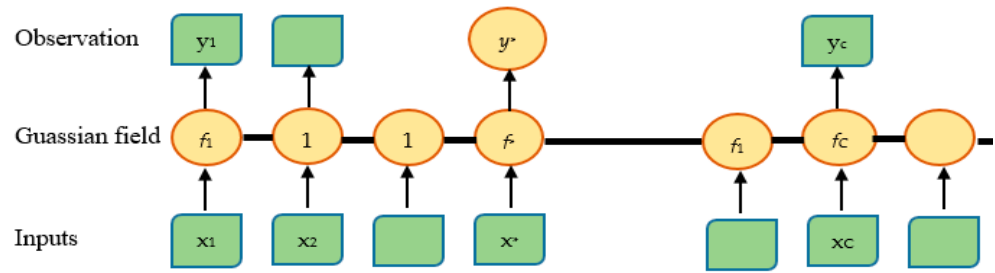


Figure 4. Structure of the GPR model.

Subsequently, the GPR underwent processing focusing on the Bayesian distribution function, given in Equation (2):

$$p(f|Q) = \frac{p(j)p(q|f)}{p(Q)} \tag{2}$$

Thus, $z(x, x')$ expressed in Equation (3) is the covariance function of the model:

$$z(x, x') = \partial_f^2 \exp\left\{\frac{x_i - x_j}{2k^2}\right\} \tag{3}$$

The hidden function in the equation can be expressed as Equation (4):

$$y = f(x) + e \tag{4}$$

where $f(x)$ is the hidden function and e is the Gaussian noise. In GPR computing, the hidden function is represented as a random variable, while the divergence between x and x' approaches zero, indicating that the function reaches the true function $z(x)$. Thus, Equation (4) is modified to Equation (5) through noise values:

$$q(x, x') = \partial_f^2 \exp\left\{\frac{x_i - x_j}{2k^2}\right\} + \partial_n^2 \alpha(x, x') \tag{5}$$

where ∂_f^2 is the variance, and $\alpha(x, x')$ is the alpha function. Accordingly, the predicted function is given in Equation (6):

$$y = f(x) + N(0, \partial_n^2) \tag{6}$$

Finally, the covariance function $z(x, x')$ is expressed by matrix 'Z':

$$Z = \begin{pmatrix} q(x_1, x_1) & q(x_1, x_2) & \dots & q(x_1, x_n) \\ \dots & \dots & \dots & \dots \\ q(x_n, x_2) & q(x_n, x_2) & \dots & q(x_n, x_n) \end{pmatrix} \tag{7}$$

3.2. SVR Model

SVR is an adaptation of the SVM model originally designed for classification tasks, now tailored for regression analysis. It constructs a plane or hyperplane, aiming at minimizing the sample's overall deviation from the hyperplane. Its primary goal is to reduce the error by developing a regression function that maximizes the fit between data points and a curve [55]. Figure 5 presents the architecture of SVR. The process is explained as a constrained optimization issue, as expressed [56]:

$$\min\left(\frac{1}{2} \|w\|^2 + C \sum_{i=1}^n (\xi_i^* + \xi_i)\right) \tag{8}$$

$$\text{subject to : } \left\{ \begin{array}{l} y_i - \langle w, x_i \rangle - b \leq \varepsilon + \xi_i^* \\ \langle w, x_i \rangle + b - y_i \leq \varepsilon + \xi_i^* \end{array} \right\} \quad (9)$$

where x_i is the i th input variable, y_i is the target, and w is the weight vector. ξ_i is defined as the distance between the boundaries, and C is the penalty coefficient. Therefore, the regression function of the SVR model is given in Equation (10):

$$f(x) = w\phi(x) + b \quad (10)$$

where $\phi(x)$ defines the nonlinear mapping relation, w and b are the weight vector and bias, respectively.

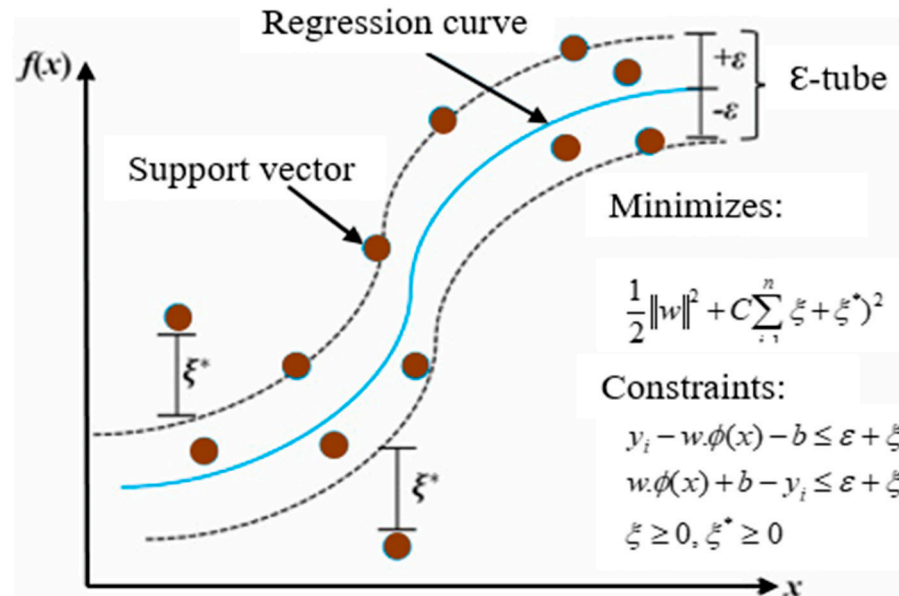


Figure 5. Structure of the SVR model.

3.3. IEPSO

IEPSO was developed by Lv et al. [57] to enhance personal–global information analysis and global optimization efficiency. It is an extension of PSO. Equation (11) defines each particle’s updated position and velocity in the solution space:

$$V_{ij}^{k+1} = wV_{ij}^k + \underbrace{c_1r_1(p_{bestij}^k - X_{ij}^k)}_{\text{Standard PSO}} + \underbrace{c_2r_2(G_{bestij}^k - X_{ij}^k)}_{\phi_3} + c_3r_3|G_{bestij}^k - p_{ij}^k| \quad (11)$$

The terms in Equation (12) represent the conventional PSO algorithm’s updated velocity. ϕ_3 refers to the extension of PSO. Moreover, IEPSO allows for more than just one-way information transmission among the global and individual best particles. The value of c_3 is decided using two criteria. If c_3 is assumed to be a constant, c_3 equals 2. Equation (12) is used to determine c_3 :

$$c_3 = k \left[(c_{3i} - c_{3j}) \times \frac{t}{t_{\max}} \right] \quad (12)$$

where k is the controlling factor with a value of -1 and $+1$, C_{3i} is the first value of c_3 , c_{3j} is the last value of c_3 , t is the number of iterations, and t_{\max} is the highest iteration time.

3.4. IEPANN

IEPANN is an ensemble technique developed using the optimization of ANNs and IEPHO to predict the performance of composite U-shaped specimens at the training and verification phases. The learning approach of the IEPANN is expressed in Equations (11) and (12) and schematically depicted in Figure 6. This approach is utilized to train the artificial neural network through IEPHO. The process starts with the generation of random particles, with their positions representative of the ANN’s weight and bias. The hybrid technique involves training according to primary weight and bias and then determining the mean square error (MSE) between the experimental and target variables. The model’s performance was improved by gradually altering the particles’ positions and lowering the MSE at every iteration. P_{best} and G_{best} were selected to evaluate and update new velocities at every iteration. Optimization is performed based on this protocol until the termination criteria are obtained. Stopping could be based on a lower MSE or ultimate iteration count.

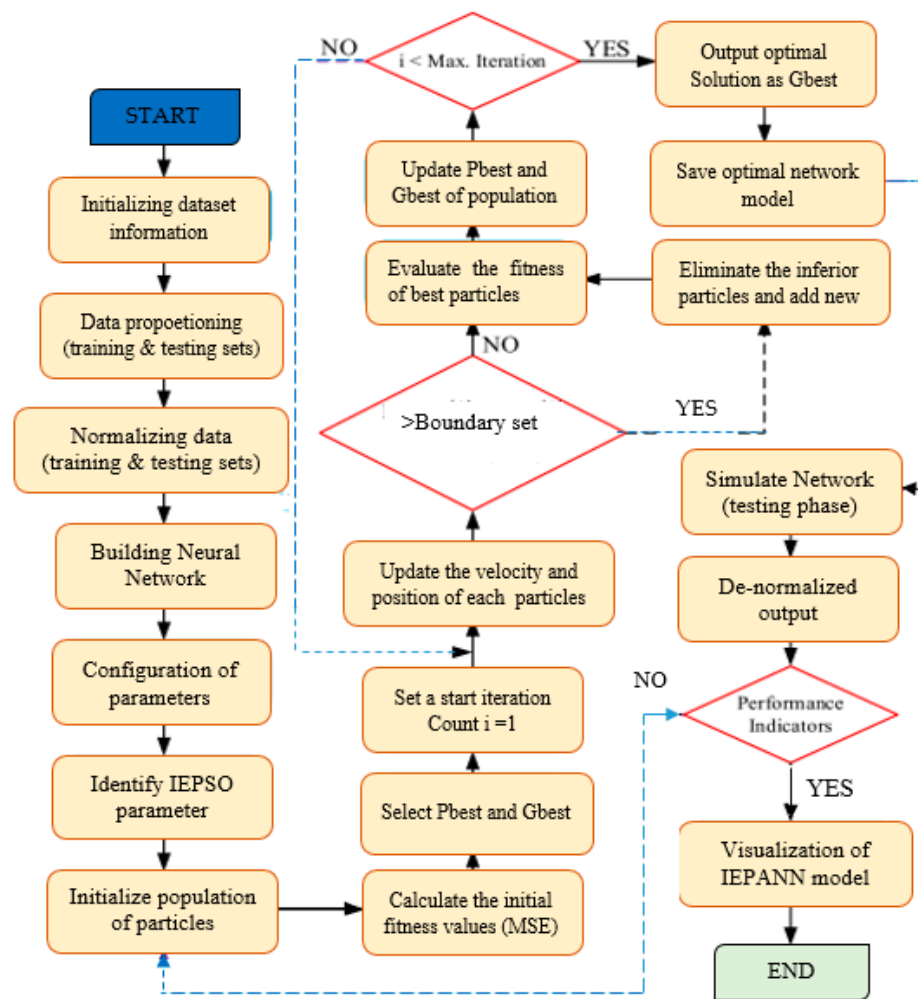


Figure 6. Systematic structure of the IEPANN model.

3.5. Model Performance Matrix

Table 2 presents the evaluation matrix for checking the performance of the developed model, including commonly used matrix parameters for physical dimensionless quantities. These dimensionless quantities are sometimes expressed in percentages, degrees, etc. [58]. The matrix includes Nash–Sutcliffe efficiency (NSE), mean absolute error (MAE), root mean square error (RMSE), and percentage bias (PBIAS). The dataset was normalized to improve

its integrity and eliminate inconsistencies between datasets. Equation (13) was used to normalize the datasets:

$$y_{norm} = \frac{y - y_{min}}{y_{max} - y_{min}} \tag{13}$$

where y_{norm} represents the normalized data, and y , y_{min} , and y_{max} are the observed, maximum, and minimum data, respectively.

Table 2. Evaluation matrix.

Matric	Formula	Description
NSE	$1 - \frac{\sum_{i=1}^n (N_{obsi} - N_{prei})^2}{\sum_{i=1}^n (N_{obsi} - N_{obsi})^2}$	The NSE defines the fitness of the model. It has values between $-\infty$ and 1. NSE = 1 indicates the highest prediction accuracy and vice versa.
MAE	$MAE = \frac{1}{2} \sum_{i=1}^n m_i - p_i $	MAE has a value between $0 < MAE < \infty$, indicating the MAE value between the measured and target values.
RMSE	$\sqrt{\frac{1}{n} \sum_{i=1}^n (q_i - p_i)^2}$	Describing the difference between the experimental and target values, a lower RMSE value indicates good performance.
PBIAS	$\left[\frac{\sum_{i=1}^n (y_i - o_i)}{\sum_{i=1}^n o_i} \right] \times 100$	The PBIAS is used to calculate the average tendency of the computed values, bigger or smaller than the experimental results.

4. Results and Discussion

ML Model Results

After the sensitivity analysis where the parameters' relevance was evaluated, the dataset was grouped into 70% and 30% for training and verification. The data were also normalized between 0 and 1 to prevent data with greater values from overriding those with lower values, as recommended [59]. MATLAB 2021 was used in this study to train the three machine learning models (IEPANN, SVR, and GPR). IEPANN is a hybrid model that was formed by employing IEPHO to optimize ANN models. Training the IEPANN model involved two stages (see Figure 6). The first stage involved developing an ANN model, and in the second stage, IEPHO was used to optimize the ANN technique's weights and bias. Correct model structure is essential for developing any machine learning technique like an ANN model. For developing the ANN model, several model structures were developed, and the structure with five input parameters, seven hidden neurons, and a single output layer trained with the Levenberg–Marquardt algorithm was found to be the optimum model structure with the least mean square error and lowest R^2 value. The optimum result was obtained using *Sigmoid* and *Purlin* functions, respectively, in the hidden and output layers of the ANN model. After obtaining the optimum ANN structure, the model was used to optimize the weight and bias of the ANN models during the iteration process. The population size, inertia weight, and the stopping criteria for the IEPHO were enhanced in the ANN. The IEPHO parameters optimized include swamp size, inertia weight, and termination criteria. The inertia weight was $\omega = 0.729$, and its damping ratio was 1, while the lower and upper bound velocities were -5 and 5 , respectively, obtained using Equation (14) [60]. A trial-and-error procedure was employed with a population size of 50–500 with an increment of 50. The model concert increases by changing the positions of the particle while the MSE reduces a little at each iteration:

$$V_1 = \lambda\phi_1, V_2 = \lambda\phi_2, \lambda = \frac{2}{\phi - 2\sqrt{\phi^2 - 4\phi}}, \phi = \phi_1 + \phi_2 \tag{14}$$

Similarly, for the classical single models, Bayesian search optimization algorithms were used to train several SVR and GPR models using different hyperparameters (kernel

functions, kernel scale, basis function, sigma values, learning rate, and epsilon value), and only optimum models are reported in this study. The MSE metric was used for selecting the optimum value. Several models were developed using different parameters and the model structure with least MSE value was selected as the optimum structure. Two single ML models (SVR and GPR) were developed to validate the performance accuracy of the hybrid model (IEPANN). All three models were evaluated using RMSE, MAE, Nash NSE, and PBIAS. A model is considered excellent when the R^2 value > 0.75 [61] and error metrics are close to zero. A PBIAS value close to zero indicates high accuracy and stability. The best SVR model was obtained using a Gaussian kernel and kernel scale of 8.9, while the best GPR model was obtained with the isotropic exponential kernel. The modeling results for the IEPANN, SVR, and GPR models are summarized in Table 3.

Table 3. Performance of single models.

Model	Training				Verification			
	NSE	RMSE	MAE	PBIAS	NSE	RMSE	MAE	PBIAS
SVR	0.9983	0.0177	0.0139	0.0248	0.9934	0.0101	0.0065	0.0705
GPR	0.9983	0.0174	0.0135	0.0242	0.9961	0.0078	0.0050	0.0536
IEPANN	0.9999	0.0031	0.0010	0.0018	0.9996	0.0025	0.0009	0.0095

From the results, it can be noted that all the models predicted the failure strength with excellent results, with $NSE > 0.75$, PBIAS, and normalized error metrics (MAE and RMSE) close to zero. The IEPANN outperformed the classical models, with an NSE value of 99.99% in the training and 99.96% in the verification phase. The IEPANN similarly indicated its superiority over SVR and GPR in terms of MAE, RMSE, and PBIAS values. The IEPANN modelled the failure strength with RMSE, MAE, and PBIAS values of 0.0025, 0.0009, and 0.0095 respectively, in the verification stage. The normalized RMSE, MAE and PBIAS values of the IEPANN model were (0.0076, 0.0056, and 0.0610) and (0.0053, 0.0041, 0.0041) lower compared with the SVR and GPR models, respectively. The IEPANN also demonstrated better stability, with as little as 0.03% difference between the NSE values in the training and verification stages. Several studies have reported improved ANN performance when PSO was used to optimize ANN parameters [62]. The IEPANN derives its superiority by analytically optimizing the ANN parameters (bias and weights) using the IEPSO algorithm by updating the particles' position. Scatter plots (Figure 7) showing the models' goodness of fit were also used to compare the performance of the IEPANN model with the single classical models (SVR and GPR). It can be seen that the data are more compacted along the chart bisector in Figure 7c, indicating better agreement between the observed and predicted failure strength for the IEPANN technique. All the models were also compared using a violin plot (Figure 8) including boxplots, interquartile ranges, and distribution plots. All the models mimicked the experimental data well, indicating the models' suitability for predicting failure strength. The findings for the developed models were compared with results found in the literature for small datasets utilized with AI-based models, as summarized in Table 4; those models predicted the concrete's properties with high R^2 values [63–66].

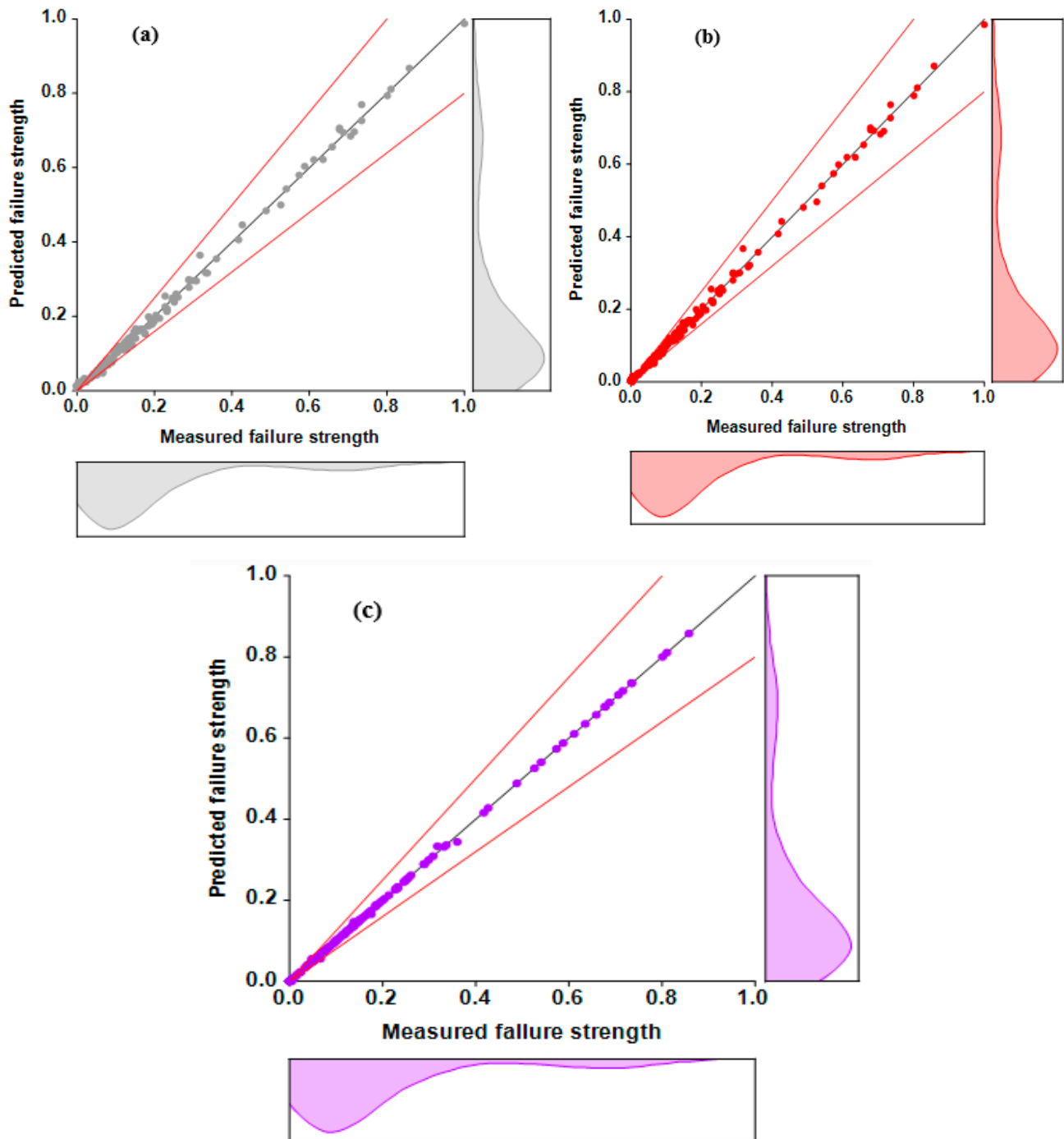


Figure 7. Scatter plots showing the measured and predicted values: (a) SVR; (b) GPR; and (c) IEPANN.

Table 4. Comparison of results with existing developed AI models from the literature.

Reference	AI-Based Model	Material	Input Variables	Datasets	R ²
Boga et al. [66]	ANN and ANFIS	concrete	4	162	0.98
Alfuhaid [64]	ANN, ANFIS, SVM, and ELM	concrete	8	105	0.959
Pirachatprecha et al. [65]	ANN	HPC	8	86	0.98
Hoang et al. [63]	ANN and ANFIS	concrete	4	162	0.982

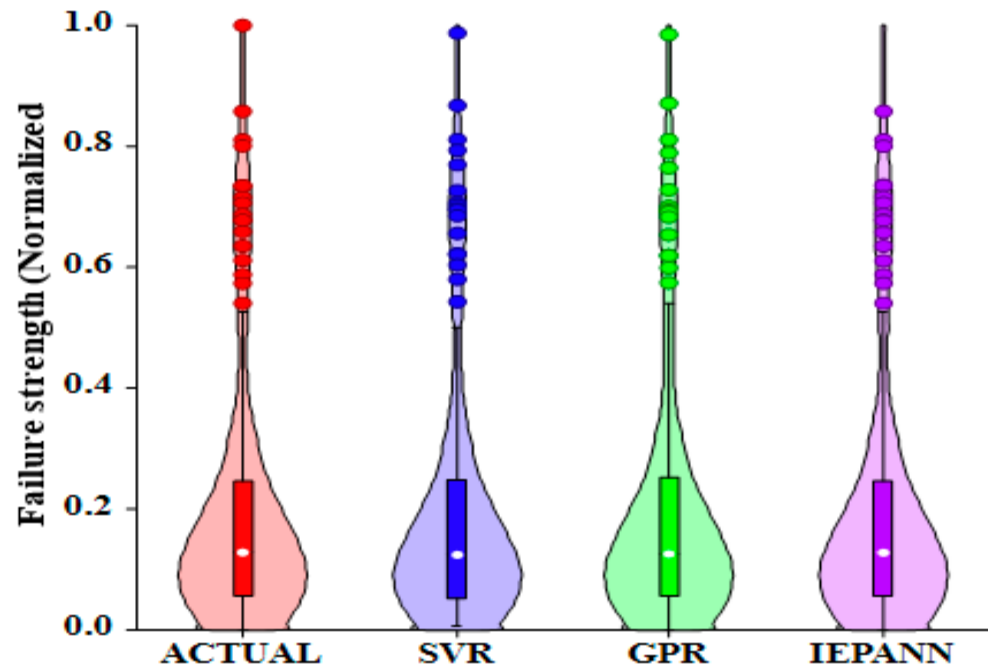


Figure 8. Violin plots comparing the experimental failure strength data and the other three models.

The RMSE, standard deviation, and correlation coefficients of the experimental data and the three developed machine learning models are compared graphically in Figure 9, using Taylor plots. All the models had correlation coefficients > 0.99. The standard deviations of the models were almost similar to that of the data, eliminating the overfitting issues in the models [67]. The RMSE values were also less than 0.05 (normalized), indicating a high level of accuracy for the models in predicting failure strength.

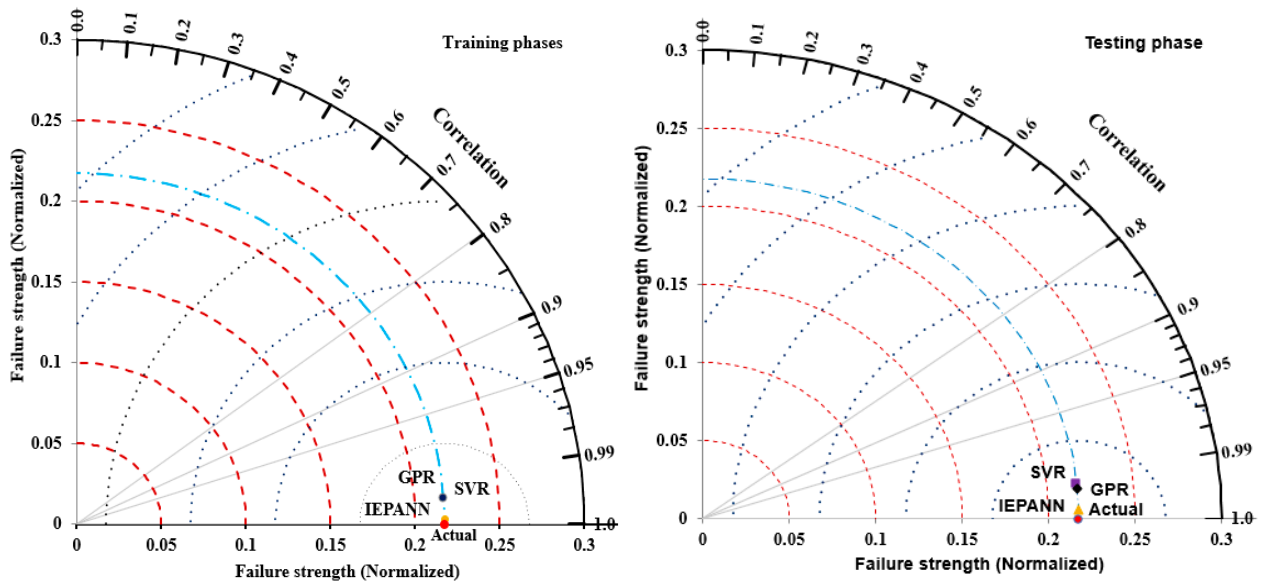


Figure 9. Taylor plots comparing the experimental failure strength data and the other three models.

5. Statistical Analysis

5.1. Weibull Distribution

Weibull distribution analysis is a statistical technique commonly used for solving scientific problems, which was firstly established by Wallodi Weibull. The method involves shape and scale factors for reliability investigation. Fatigue and dynamic properties can be evaluated using two-parameter Weibull distribution, as reported [11,68]. The Weibull distribution function is characterized by rises or falls in concrete properties [69]. The two-parameter distribution function was applied to determine the variations in impact strength data obtained in this study. The probability function $f(P)$ to evaluate the impact strength data is given Equation (15) [70]:

$$f(p) = \frac{\tau}{z - x_0} \left[\frac{n - x_0}{z - x_0} \right]^{\tau-1} * Exp \left\{ - \left[\frac{x - x_0}{z - x_0} \right]^\tau \right\} \quad z \leq x \leq \infty \quad (15)$$

Integrating Equation (15) to obtain the random variable distribution function $f(P_r)$:

$$f(P_r) = p(x \leq x_r) = 1 - Exp \left\{ - \left[\frac{x - x_0}{z - x_0} \right]^\tau \right\} \quad (16)$$

where x is the value of the random variable P , (τ, z) ; z is the shape parameter, τ is the scale factor, and x_0 is the location parameter: $x \geq x_0$, $\tau > 0$, and $z \geq x_0$.

Let x_0 be the minimum life span of a composite U-shaped specimen under multiple-impact load testing. Equation (17) translates the survival probability function $f(N_r)$:

$$f(N_r) = 1 - Exp \left\{ - \left[\frac{x - x_0}{z - x_0} \right]^\tau \right\} \quad (17)$$

Computing the log of Equation (17) twice gives:

$$Ln \left\{ Ln \left[\frac{1}{F(X_r)} \right] \right\} = \tau Ln(x) - \tau Ln(z) \quad (18)$$

Therefore, Equation (18) was applied to check the suitability of the data for the composite U-shaped specimens and their agreement with the two-parameter function, analyzing Equation (18) as a linear function relating to a straight-line equation ($y = bx + c$) to obtain τ , $\tau Ln(z)$, and R^2 . The survival function $f(N_r)$ is stated in Equation (19) [71,72]:

$$f(N_r) = P_j = 1 - \frac{Y}{J + 1} \quad (19)$$

where Y represents the impact times in rising order and J is the total number of test samples in a particular group.

The impact data are assumed to follow the two-parameter function when the linear function between $Ln(1/P_j)$ and $Ln(x)$ is established [71,72]. Figure 10 depicts the data distribution for all groups, presented in Weibull charts. The shape parameter, scale factor, and R^2 for (N1) and (N2) are presented in Table 4. As observed in Table 5, the R^2 values for both N1 and N2 of all the test specimens under the two scenarios were greater than 0.9, except for NC_{SS}-UHPC, which was attributed to the poor interfacial bond capacity; all the specimens in this group failed with few drops. Thus, according to the results obtained, the two-parameter method can be utilized to evaluate the impact data of composite U-shaped test specimens. The results are presented in Table 4.

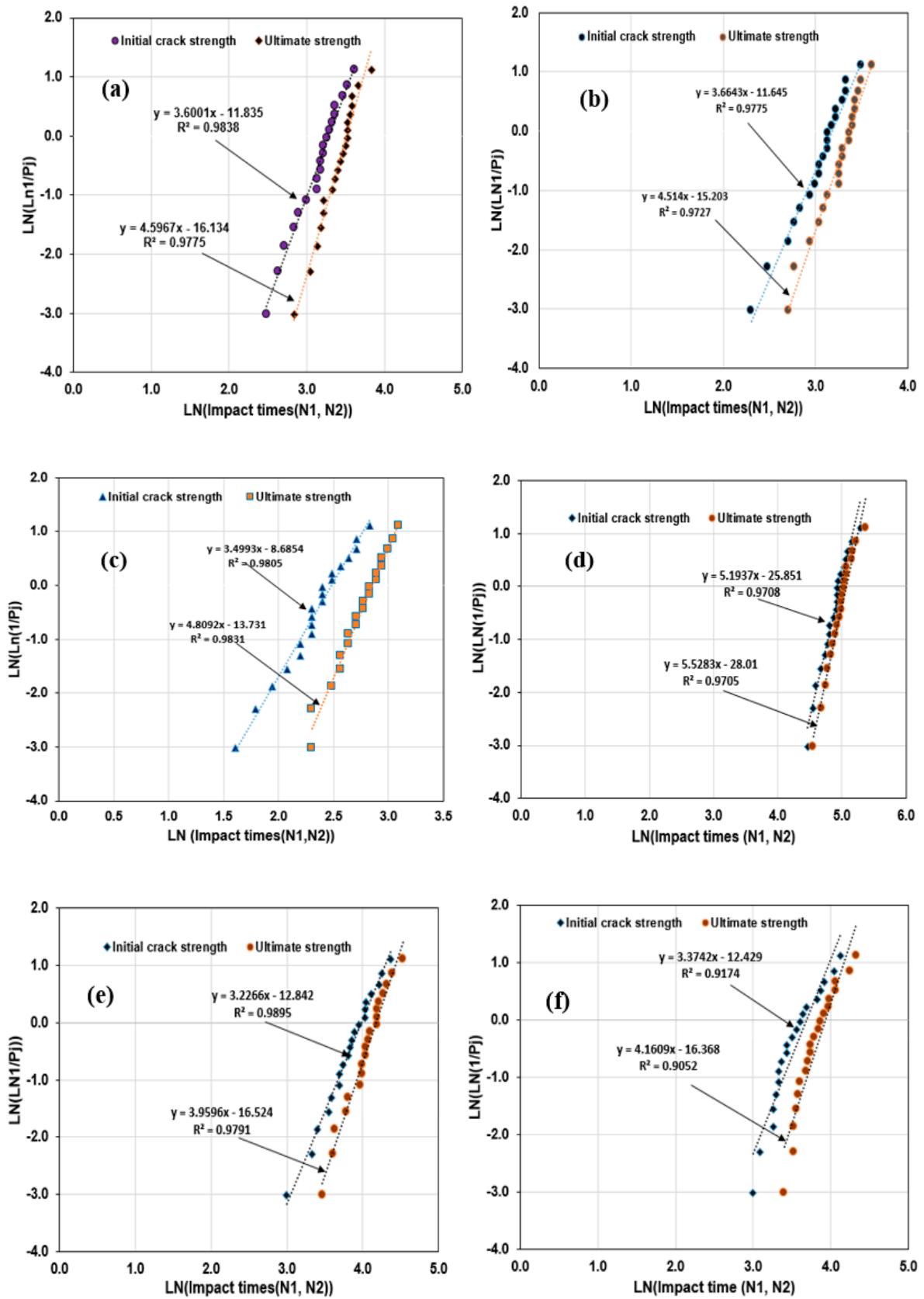


Figure 10. Weibull distribution analysis of impact data for (a) reference NC, (b) NC_{NF} -UHPC, (c) NC_{GS} -UHPC, (d) NC_{NS} -PUPC, (e) NC_{GS} -PUPC, and (f) NC_{SS} -PUPC.

Table 5. Results of Weibull distribution analysis.

Specimen ID	Impact Strength	τ	$\tau \text{Ln}(z)$	(z)	R^2
NC reference	N1	3.6	11.835	27	0.9838
	N2	4.596	16.134	34	0.9775
NC _{NB} -UHPC	N1	3.664	11.645	24	0.9775
	N2	4.515	15.203	29	0.9727
NC _{GB} -UHPC	N1	3.499	8.685	12	0.9805
	N2	4.809	13.731	17	0.9831
NC _{NB} -PUPC	N1	5.194	25.851	144	0.9708
	N2	5.528	28.01	157	0.9705
NC _{GB} -UUPC	N1	3.227	12.847	54	0.9895
	N2	3.959	16.524	65	0.9791
NC _{SM} -PUPC	N1	3.374	12.429	39	0.9174
	N2	4.161	16.368	52	0.9052

5.2. Reliability Analysis

According to the findings in Section 3.1, the impact times and different survival probabilities were evaluated, referred to as the “reliability analysis”. The failure probability (P') for the various impact times achieved for each test specimen was determined using Equation (20) [70,72]:

$$N = z \{ \text{Ln}(1 - P') \}^{\frac{1}{\tau}} \tag{20}$$

where N is the total number of impacts, P' is the failure probability, and z and τ are the scale and shape factors, respectively. The design survival probability (λ) was determined using Equation (21):

$$\lambda = 1 - P' \tag{21}$$

Table 6 summarizes the number of impact blows on the composite U-shaped specimens computed for different survival probabilities (SPs), as also presented in Figure 10. The design impact strength of the composite U-shaped specimens was measured only at a low probability value that cracks failure would happen. Figure 11 shows that the number of impacts ($N1$ and $N2$) reduced as the survival probability increased. For instance, in reference NC specimen at 80% SP, reflecting 20% failure probability, the impact times at the $N1$ and $N2$ stages were 18 blows and 24 blows, respectively, which appeared to be lower than the mean number of impacts in the group. This showed that approximately 80% of the reference specimens were able to sustain these drops without fracture. Similarly, at 80%SP, NC_{NF}-UHPC and NC_{NF}-PUPC were able to withstand 16 and 107 drops prior to the occurrence of the initial crack, and 21 and 117 blows before ultimate failure, respectively. This finding agrees with the findings in previous studies [50]. However, some test specimens showed an initial crack strength less than the design strength achieved in the reliability analysis.

Overall, the design impact strength of the composite U-shaped specimens increased with lower survival probability (Figure 11a–f). Greater design impact strength can be obtained at low survival probability. Thus, this analysis result is near to the findings from experimental testing.

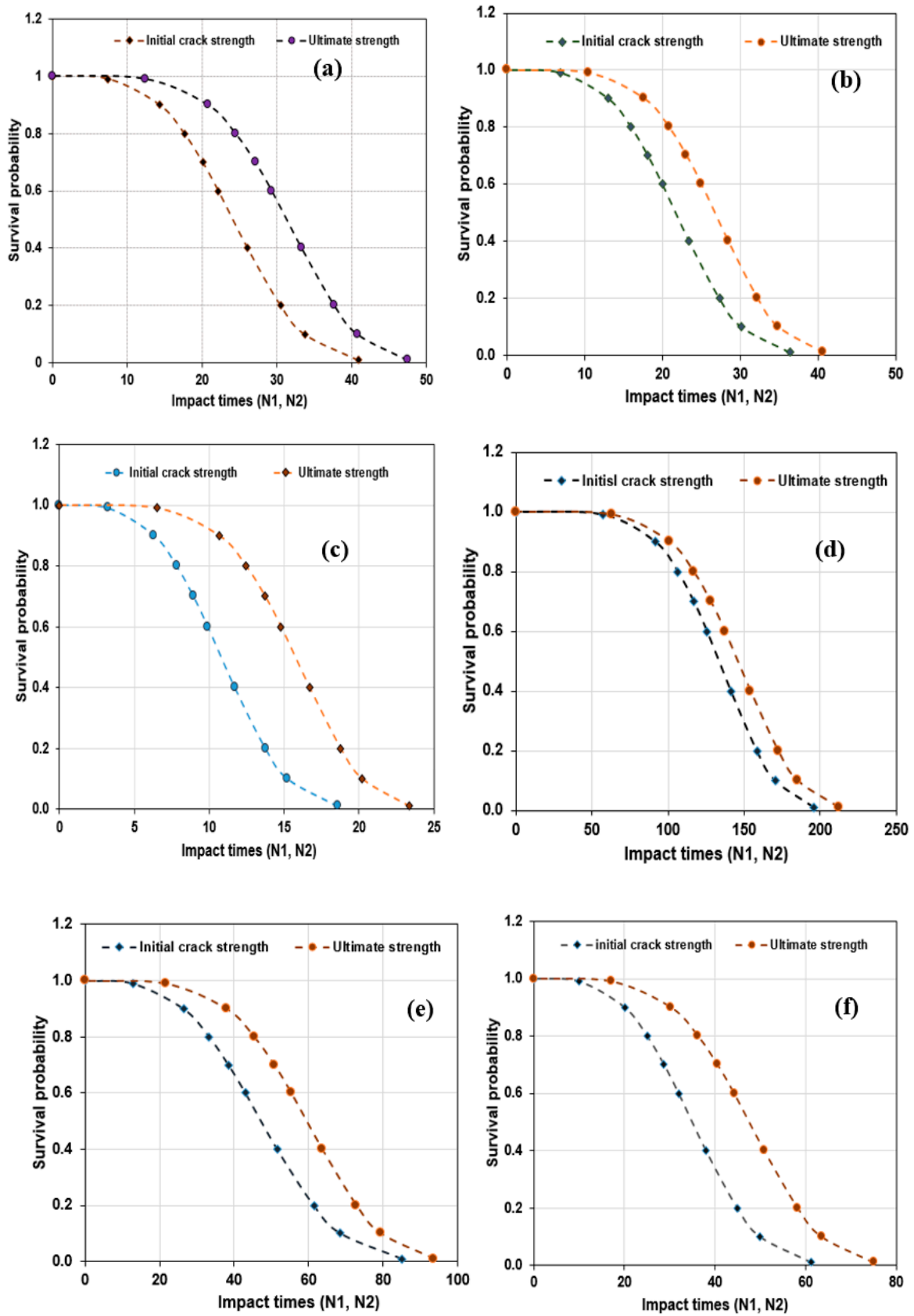


Figure 11. Reliability analysis of impact data for (a) reference NC, (b) NC_{NB}-UHPC, (c) NC_{GB}-UHPC, (d) NC_{NB}-PUPC, (e) NC_{GB}-PUPC, and (f) NC_{SM}-PUPC.

Table 6. Impact strength of test samples at different survival probabilities.

Specimen ID	Impact Strength	Survival Probability					
		$\lambda = 0.01$	$\Lambda = 0.2$	$\lambda = 0.6$	$\lambda = 0.8$	$\lambda = 0.9$	$\lambda = 0.99$
NC reference	N1	41	30	22	18	14	7
	N2	47	37	29	24	21	12
NC _{NF} -UHPC	N1	36	27	20	16	13	7
	N2	41	32	25	21	18	7
NC _{GS} -UHP	N1	19	14	10	8	6	3
	N2	23	19	15	12	11	6
NC _{NF} -PUPC	N1	195	158	126	107	91	57
	N2	212	172	138	117	101	63
NC _{GS} -PUPC	N1	85	61	43	33	26	13
	N2	94	73	55	45	38	22
NC _{SS} -PUPC	N1	62	45	32	25	20	10
	N2	75	58	44	36	30	17

6. Conclusions

This study demonstrated the efficacy of machine learning models in forecasting the ultimate strength of composite concrete retrofitted with PU grout under impact load. This research involved the use of classical and hybrid techniques, including GPR, SVR, and IEPANN models. The analysis was performed through calibration and verification phases, providing a comprehensive assessment of the models' performance and generalization capabilities. Moreover, reliability analysis was performed on the impact data to evaluate the design impact strength of the composite U-shaped specimens. The findings of this study can be summarized as follows:

- All models revealed high prediction accuracy, achieving NSE values above acceptable thresholds, with NSE greater than 90% across the dataset. Performance indicators such as RMSE (ranging from 0.0013 to 0.017), PBIAS (from 0.0018 to 0.0248), and MAE (from 0.001 to 0.0139) were all within permissible limits at the testing stage. Additionally, similar results were obtained at the verification stage. Across the entire dataset, the ratio of observed and predicted strength values was nearly equal to 1 for all the developed models.
- Among the developed models, the hybrid IEPANN appeared to be the most effective model, demonstrating the highest NSE value of 0.999 and the lowest RMSE, PBIAS, and MAE values of 0.0013, 0.0018, and 0.001, respectively, compared with the nonlinear techniques. However, other individual models demonstrated high prediction skills.
- The initial cracking strength and flexural stress of the U-shaped samples were the leading factors contributing to the prediction of the output parameter, with correlation values of +1 and 0.88, respectively, based on the Pearson correlation matrix. This high correlation with failure strength shows the significant influence of these parameters on the model's estimation.
- The statistical analysis of the dataset of composite U-shaped specimens under two scenarios followed the two-parameter Weibull distribution function; hence, reliability analysis revealed that the number of impacts (N1 and N2) reduced as the survival probability increased. At 80% survival probability, NC_{NF}-UHPC and NC_{NF}-PUPC specimens were able to withstand 16 and 107 blows before the first crack, and 21 and 117 blows before complete failure, respectively, which agreed with the experimental results.

In conclusion, this research offers important new information about the suitability of ML methods for forecasting the failure strength and determining the design impact strength of composite samples under multiple impact loads. This research can avert the need for high-cost experiment programs and save time. The findings can illuminate future research and serve as a guide for engineering practice. Future studies could also employ the applicability of other machine learning techniques, such as XGB and DNN models.

Author Contributions: S.I.H.: conceptualization, writing—original draft, writing—review and editing, formal analysis; Y.E.I.: supervision, investigation, funding acquisition, formal analysis; I.K.U.: investigation, visualization, methodology, investigation, data curation, writing—review and editing. All authors have read and agreed to the published version of the manuscript.

Funding: The APC was funded by the Structures and Materials Laboratory (S&M Lab) of the College of Engineering, Prince Sultan University, Riyadh, Saudi Arabia.

Data Availability Statement: The original contributions presented in the study are included in the article. Further inquiries can be directed to the corresponding author.

Acknowledgments: The authors greatly acknowledge the financial support of this research by the Structure and Materials (S&M) Lab of Prince Sultan University for funding the APC.

Conflicts of Interest: The authors declare no conflicts of interest.

References

1. Beushausen, H.; Torrent, R.; Alexander, M.G. Performance-based approaches for concrete durability: State of the art and future research needs. *Cem. Concr. Res.* **2019**, *119*, 11–20. [[CrossRef](#)]
2. Alexander, M.; Beushausen, H. Durability Durability, service life prediction, and modelling for reinforced concrete structures—review and critique. *Cem. Concr. Res.* **2019**, *122*, 17–29. [[CrossRef](#)]
3. Beushausen, H.; Höhlig, B.; Talotti, M. The influence of substrate moisture preparation on bond strength of concrete overlays and the microstructure of the OTZ. *Cem. Concr. Res.* **2017**, *92*, 84–91. [[CrossRef](#)]
4. Espeche, A.D.; León, J. Estimation of bond strength envelopes for old-to-new concrete interfaces based on a cylinder splitting test. *Constr. Build. Mater.* **2010**, *25*, 1222–1235. [[CrossRef](#)]
5. Julio, E.N.; Branco, F.A.; Silva, V.D. Concrete-to-concrete bond strength. Influence of the roughness of the substrate surface. *Constr. Build. Mater.* **2004**, *18*, 675–681. [[CrossRef](#)]
6. Yang, Y.; Du, X.; Yu, Y.; Pan, Y. Experimental study on the seismic performance of composite columns with an ultra-high-strength concrete-filled steel tube core. *Adv. Struct. Eng.* **2019**, *23*, 794–809. [[CrossRef](#)]
7. Hung, C.-C.; Hsiao, H.-J.; Shao, Y.; Yen, C.-H. A comparative study on the seismic performance of RC beam-column joints retrofitted by ECC, FRP, and concrete jacketing methods. *J. Build. Eng.* **2022**, *64*, 105691. [[CrossRef](#)]
8. Al-Nimry, H.S.; Al-Rabadi, R.A. Axial-Flexural Interaction in FRP-Wrapped RC Columns. *Int. J. Concr. Struct. Mater.* **2019**, *13*, 53. [[CrossRef](#)]
9. Ouyang, L.-J.; Chai, M.-X.; Song, J.; Hu, L.-L.; Gao, W.-Y. Repair of thermally damaged concrete cylinders with basalt fiber-reinforced polymer jackets. *J. Build. Eng.* **2021**, *44*, 102673. [[CrossRef](#)]
10. Haruna, S.I.; Ibrahim, Y.E.; Han, Z.; Farouk, A.I.B. Flexural Response of Concrete Specimen Retrofitted with PU Grout Material: Experimental and Numerical Modeling. *Polymers* **2023**, *15*, 4114. [[CrossRef](#)]
11. Haruna, S.; Zhu, H.; Ibrahim, Y.E.; Shao, J.; Adamu, M.; Ahmed, O.S. Impact resistance and flexural behavior of U-shaped concrete specimen retrofitted with polyurethane grout. *Case Stud. Constr. Mater.* **2023**, *19*, e02547. [[CrossRef](#)]
12. Nataraja, M.; Dhang, N.; Gupta, A. Statistical variations in impact resistance of steel fiber-reinforced concrete subjected to drop weight test. *Cem. Concr. Res.* **1999**, *29*, 989–995. [[CrossRef](#)]
13. Song, P.; Wu, J.; Hwang, S.; Sheu, B. Assessment of statistical variations in impact resistance of high-strength concrete and high-strength steel fiber-reinforced concrete. *Cem. Concr. Res.* **2004**, *35*, 393–399. [[CrossRef](#)]
14. Nia, A.A.; Hedayatian, M.; Nili, M.; Sabet, V.A. An experimental and numerical study on how steel and polypropylene fibers affect the impact resistance in fiber-reinforced concrete. *Int. J. Impact Eng.* **2012**, *46*, 62–73.
15. AlAhmed, Y.S.; Hassan, N.M.; Bahroun, Z. Significance of Sandwich Panel's Core and Design on Its Impact Resistance under Blast Load. *J. Compos. Sci.* **2023**, *7*, 44. [[CrossRef](#)]

16. Al-Shawafi, A.; Zhu, H.; Haruna, S.; Bo, Z.; Laqsum, S.A.; Borito, S.M. Impact resistance of ultra-high-performance concrete retrofitted with polyurethane grout material: Experimental investigation and statistical analysis. *Structures* **2023**, *55*, 185–200. [[CrossRef](#)]
17. Su, Q.; Wu, H.; Fang, Q. Calibration of KCC model for UHPC under impact and blast loadings. *Cem. Concr. Compos.* **2022**, *127*, 104401. [[CrossRef](#)]
18. Abid, S.R.; Abdul-Hussein, M.L.; Ayoob, N.S.; Ali, S.H.; Kadhum, A.L. Repeated drop-weight impact tests on self-compacting concrete reinforced with micro-steel fiber. *Heliyon* **2020**, *6*, e03198. [[CrossRef](#)]
19. Abid, S.R.; Hussein, M.L.A.; Ali, S.H.; Kazem, A.F. Suggested modified testing techniques to the ACI 544-R repeated drop-weight impact test. *Constr. Build. Mater.* **2020**, *244*, 118321. [[CrossRef](#)]
20. Anas, S.; Alam, M.; Tahzeeb, R. Impact response prediction of square RC slab of normal strength concrete strengthened with (1) laminates of (i) mild-steel and (ii) C-FRP, and (2) strips of C-FRP under falling-weight load. *Mater. Today Proc.* **2022**, *87*, 9–19. [[CrossRef](#)]
21. Fan, W.; Chen, Y.; Li, J.; Sun, Y.; Feng, J.; Hassanin, H.; Sareh, P. Machine learning applied to the design and inspection of reinforced concrete bridges: Resilient methods and emerging applications. *Structures* **2021**, *33*, 3954–3963. [[CrossRef](#)]
22. Dang, H.V.; Trestian, R.; Bui-Tien, T.; Nguyen, H.X. Probabilistic method for time-varying reliability analysis of structure via variational bayesian neural network. *Structures* **2021**, *34*, 3703–3715. [[CrossRef](#)]
23. Haruna, S.I.; Malami, S.I.; Adamu, M.; Usman, A.G.; Farouk, A.; Ali, S.I.A.; Abba, S.I. Compressive Strength of Self-Compacting Concrete Modified with Rice Husk Ash and Calcium Carbide Waste Modeling: A Feasibility of Emerging Emotional Intelligent Model (EANN) Versus Traditional FFNN. *Arab. J. Sci. Eng.* **2021**, *46*, 11207–11222. [[CrossRef](#)]
24. Farouk, A.I.B.; Jinsong, Z. Prediction of Interface Bond Strength Between Ultra-High-Performance Concrete (UHPC) and Normal Strength Concrete (NSC) Using a Machine Learning Approach. *Arab. J. Sci. Eng.* **2022**, *47*, 5337–5363. [[CrossRef](#)]
25. Li, Z.; Long, Z.; Lei, S.; Zhang, T.; Liu, X.; Kuang, D. Predicting the glass formation of metallic glasses using machine learning approaches. *Comput. Mater. Sci.* **2021**, *197*, 110656. [[CrossRef](#)]
26. Islam, M.; Hossain, B.; Akhtar, N.; Moni, M.A.; Hasan, K.F. CNN Based on Transfer Learning Models Using Data Augmentation and Transformation for Detection of Concrete Crack. *Algorithms* **2022**, *15*, 287. [[CrossRef](#)]
27. Roudsari, S.S.; Ungureanu, L.M.; Soroushnia, S.; Abu-Lebdeh, T.; Petrescu, F.I.T. Optimization of Fiber-Reinforced Polymer Bars for Reinforced Concrete Column Using Nonlinear Finite Element Algorithms. *Algorithms* **2021**, *15*, 12. [[CrossRef](#)]
28. Yazici, S.; Sezer, G.I.; Sezer, A. Prediction of Impact Resistance Properties of Concrete Using Radial Basis Function Networks. *Acta Phys. Pol. A* **2017**, *132*, 1036–1040. [[CrossRef](#)]
29. Moein, M.M.; Saradar, A.; Rahmati, K.; Rezakhani, Y.; Ashkan, S.A.; Karakouzian, M. Reliability analysis and experimental investigation of impact resistance of concrete reinforced with polyolefin fiber in different shapes, lengths, and doses. *J. Build. Eng.* **2023**, *169*, 106262. [[CrossRef](#)]
30. Mane, K.M.; Chavan, S.P.; Salokhe, S.A.; Nadgouda, P.A.; Kumbhar, Y.D. Predicting the impact strength and chloride permeability of concrete made with industrial waste and artificial sand using ANN. *Innov. Infrastruct. Solut.* **2024**, *9*, 306. [[CrossRef](#)]
31. Palamarchuk, A.; Yudaev, P.; Chistyakov, E. Polymer Concretes Based on Various Resins: Modern Research and Modeling of Mechanical Properties. *J. Compos. Sci.* **2024**, *8*, 503. [[CrossRef](#)]
32. Li, L.; Mortazavi, M.; Far, H.; El-Sherbeeny, A.M.; Fini, A.A. Simulation and modeling of polymer concrete panels using deep neural networks. *Case Stud. Constr. Mater.* **2024**, *20*, e02912. [[CrossRef](#)]
33. Keshtegar, B.; Bagheri, M.; Yaseen, Z.M. Shear strength of steel fiber-unconfined reinforced concrete beam simulation: Application of novel intelligent model. *Compos. Struct.* **2019**, *212*, 230–242. [[CrossRef](#)]
34. Onyari, E.; Ikotun, B. Prediction of compressive and flexural strengths of a modified zeolite additive mortar using artificial neural network. *Constr. Build. Mater.* **2018**, *187*, 1232–1241. [[CrossRef](#)]
35. Chou, J.; Nguyen, N. Metaheuristics-optimized ensemble system for predicting mechanical strength of reinforced concrete materials. *Struct. Control. Heal. Monit.* **2021**, *28*, e2706. [[CrossRef](#)]
36. Liang, M.; Chang, Z.; Wan, Z.; Gan, Y.; Schlangen, E.; Šavija, B. Interpretable Ensemble-Machine-Learning models for predicting creep behavior of concrete. *Cem. Concr. Compos.* **2022**, *125*, 104295. [[CrossRef](#)]
37. Sharghi, E.; Nourani, V.; Zhang, Y.; Ghaneei, P. Conjunction of cluster ensemble-model ensemble techniques for spatiotemporal assessment of groundwater depletion in semi-arid plains. *J. Hydrol.* **2022**, *610*, 127984. [[CrossRef](#)]
38. Zhang, S.-Y.; Chen, S.-Z.; Jiang, X.; Han, W.-S. Data-driven prediction of FRP strengthened reinforced concrete beam capacity based on interpretable ensemble learning algorithms. *Structures* **2022**, *43*, 860–877. [[CrossRef](#)]
39. Pan, L.X.; Lehký, D.; Novák, D.; Cao, M. Sensitivity Analysis for Parameters of Prestressed Concrete Bridge Using Neural Network Ensemble. In Proceedings of the 24th International Conference Engineering Mechanics 2018, Svratka, Czech Republic, 14–17 May 2018.
40. Pan, L.; Novák, L.; Lehký, D.; Novák, D.; Cao, M. Neural network ensemble-based sensitivity analysis in structural engineering: Comparison of selected methods and the influence of statistical correlation. *Comput. Struct.* **2020**, *242*, 106376. [[CrossRef](#)]

41. Farouk, A.I.B.; Zhu, J.; Ding, J.; Haruna, S. Prediction and uncertainty quantification of ultimate bond strength between UHPC and reinforcing steel bar using a hybrid machine learning approach. *Constr. Build. Mater.* **2022**, *345*, 128360. [[CrossRef](#)]
42. You, X.; Yan, G.; Al-Masoudy, M.M.; Kadimallah, M.A.; Alkhalifah, T.; Alturise, F.; Ali, H.E. Application of novel hybrid machine learning approach for estimation of ultimate bond strength between ultra-high performance concrete and reinforced bar. *Adv. Eng. Softw.* **2023**, *180*, 103442. [[CrossRef](#)]
43. Khan, A.-M.; Kee, S.-H.; Nahid, A.-A. Vision-Based Concrete-Crack Detection on Railway Sleepers Using Dense U-Net Model. *Algorithms* **2023**, *16*, 568. [[CrossRef](#)]
44. Cui, L.; Zhang, X.; Hao, H. Prediction of dynamic shear and maximum displacement of clamped reinforced concrete beams subjected to impact loading. *Int. J. Impact Eng.* **2024**, *195*, 105131. [[CrossRef](#)]
45. Bakhshi, M.; Valente, I.B.; Ramezansafat, H. New model for evaluating the impact response of steel fiber reinforced concrete subjected to the repeated drop-weight. *Constr. Build. Mater.* **2024**, *449*, 138459. [[CrossRef](#)]
46. Laqsum, S.A.; Zhu, H.; Bo, Z.; Haruna, S.I.; Al-Shawafi, A.; Borito, S.M. Static properties and impact resistance performance of U-shaped PU-modified concrete under repeated drop-weight impact load. *Arch. Civ. Mech. Eng.* **2023**, *23*, 227. [[CrossRef](#)]
47. Al-Shawafi, A.; Zhu, H.; Haruna, S.; Bo, Z.; Laqsum, S.A.; Borito, S.M. Experimental study and machine learning algorithms for evaluating the performance of U-shaped ultra-high performance reinforced fiber concrete under static and impact loads. *J. Build. Eng.* **2023**, *70*, 106389. [[CrossRef](#)]
48. Haruna, S.I.; Zhu, H.; Jiang, W.; Shao, J. Evaluation of impact resistance properties of polyurethane-based polymer concrete for the repair of runway subjected to repeated drop-weight impact test. *Constr. Build. Mater.* **2021**, *309*, 125152. [[CrossRef](#)]
49. Haruna, S.I.; Zhu, H.; Ibrahim, Y.E.; Shao, J.; Adamu, M.; Farouk, A.I.B. Experimental and Statistical Analysis of U-Shaped Polyurethane-Based Polymer Concrete under Static and Impact Loads as a Repair Material. *Buildings* **2022**, *12*, 1986. [[CrossRef](#)]
50. Al-Shawafi, A.; Zhu, H.; Bo, Z.; Haruna, S.; Ibrahim, Y.E.; Farouk, A.; Laqsum, S.A.; Shao, J. Bond behavior between normal concrete and UHPC and PUC layers subjected to different loading conditions coupled with fracture analysis technique. *J. Build. Eng.* **2024**, *86*, 108880. [[CrossRef](#)]
51. Haruna, S.I.; Ibrahim, Y.E.; Hassan, I.H.; Al-Shawafi, A.; Zhu, H. Bond Strength Assessment of Normal Strength Concrete–Ultra-High-Performance Fiber Reinforced Concrete Using Repeated Drop-Weight Impact Test: Experimental and Machine Learning Technique. *Materials* **2024**, *17*, 3032. [[CrossRef](#)]
52. Ali, N.M.; Farouk, A.; Haruna, S.; Alanazi, H.; Adamu, M.; Ibrahim, Y.E. Feature selection approach for failure mode detection of reinforced concrete bridge columns. *Case Stud. Constr. Mater.* **2022**, *17*, e01383. [[CrossRef](#)]
53. Liu, J.; Alexander, J.; Gu, Q.; Li, Y. Gaussian process regression-based load-carrying capacity models of corroded prestressed concrete bridge girders for fast-screening and reliability-based evaluation. *Eng. Struct.* **2023**, *285*, 116040. [[CrossRef](#)]
54. Husnain, A.; Iqbal, M.; Waqas, H.A.; El-Meligy, M.; Javed, M.F.; Ullah, R. Machine learning techniques for predicting the peak response of reinforced concrete beam subjected to impact loading. *Results Eng.* **2024**, *24*, 103135. [[CrossRef](#)]
55. Liu, Y.; Wang, L.; Gu, K. A support vector regression (SVR)-based method for dynamic load identification using heterogeneous responses under interval uncertainties. *Appl. Soft Comput.* **2021**, *110*, 107599. [[CrossRef](#)]
56. Deng, Y.; Gao, X.; Tu, T. Enhancing skeletal age estimation accuracy using support vector regression models. *Leg. Med.* **2023**, *66*, 102362. [[CrossRef](#)]
57. Lv, X.; Wang, Y.; Deng, J.; Zhang, G.; Zhang, L. Improved particle swarm optimization algorithm based on last-eliminated principle and enhanced information sharing. *Comput. Intell. Neurosci.* **2018**, *2018*, 5025672. [[CrossRef](#)]
58. Botchkarev, A. Performance metrics (error measures) in machine learning regression, forecasting and prognostics: Properties and typology. *arXiv* **2018**, arXiv:1809.03006.
59. Umar, I.K.; Gökçekuş, H.; Nourani, V. An intelligent soft computing technique for prediction of vehicular traffic noise. *Arab. J. Geosci.* **2022**, *15*, 1571. [[CrossRef](#)]
60. Poli, R.; Kennedy, J.; Blackwell, T. Particle swarm optimization. *Intell* **2007**, *1*, 33–57. [[CrossRef](#)]
61. Moriasi, D.N.; Arnold, J.G.; van Liew, M.W.; Bingner, R.L.; Harmel, R.D.; Veith, T.L. Model evaluation guidelines for systematic quantification of accuracy in watershed simulations. *Trans. ASABE* **2007**, *50*, 885–900. [[CrossRef](#)]
62. Alanazi, F.; Umar, I.K.; Haruna, S.I.; El-Kady, M.; Azam, A. Development of Artificial Intelligence Based Safety Performance Measures for Urban Roundabouts. *Sustainability* **2023**, *15*, 11429. [[CrossRef](#)]
63. Hoang, N.-D.; Chen, C.-T.; Liao, K.-W. Prediction of chloride diffusion in cement mortar using Multi-Gene Genetic Programming and Multivariate Adaptive Regression Splines. *Measurement* **2017**, *112*, 141–149. [[CrossRef](#)]
64. Fuhaid, A.; Alanazi, A.F. Prediction of Chloride Diffusion Coefficient in Concrete Modified with Supplementary Cementitious Materials Using Machine Learning Algorithms. *Materials* **2023**, *16*, 1277. [[CrossRef](#)] [[PubMed](#)]
65. Parichatprecha, R.; Nimityongskul, P. Analysis of durability of high performance concrete using artificial neural networks. *Constr. Build. Mater.* **2008**, *23*, 910–917. [[CrossRef](#)]
66. Boğa, A.R.; Öztürk, M.; Topçu, I.B. Using ANN and ANFIS to predict the mechanical and chloride permeability properties of concrete containing GGBFS and CNI. *Compos. Part B Eng.* **2013**, *45*, 688–696. [[CrossRef](#)]

67. Haruna, S.I.; Ibrahim, Y.E.; Adamu, M.; Ahmed, O.S. Determination of Final Strand Slips of Prestressed Precast Hollow-Core Slabs Subjected to Flexural Load Using Machine Learning Algorithms. *Buildings* **2023**, *13*, 2013. [[CrossRef](#)]
68. Murali, G.; Asrani, N.P.; Ramkumar, V.R.; Siva, A.; Haridharan, M.K. Impact Resistance and Strength Reliability of Novel Two-Stage Fibre-Reinforced Concrete. *Arab. J. Sci. Eng.* **2018**, *44*, 4477–4490. [[CrossRef](#)]
69. Ganesan, N.; Raj, J.B.; Shashikala, A. Flexural fatigue behavior of self compacting rubberized concrete. *Constr. Build. Mater.* **2013**, *44*, 7–14. [[CrossRef](#)]
70. Liu, F.; Meng, L.-Y.; Ning, G.-F.; Li, L.-J. Fatigue performance of rubber-modified recycled aggregate concrete (RRAC) for pavement. *Constr. Build. Mater.* **2015**, *95*, 207–217. [[CrossRef](#)]
71. Gupta, T.; Chaudhary, S.; Sharma, R.K. Mechanical and durability properties of waste rubber fiber concrete with and without silica fume. *J. Clean. Prod.* **2016**, *112*, 702–711. [[CrossRef](#)]
72. Haruna, S.I.; Zhu, H.; Shao, J. Experimental study, modeling, and reliability analysis of impact resistance of micro steel fiber-reinforced concrete modified with nano silica. *Struct. Concr.* **2022**, *23*, 1659–1674. [[CrossRef](#)]

Disclaimer/Publisher’s Note: The statements, opinions and data contained in all publications are solely those of the individual author(s) and contributor(s) and not of MDPI and/or the editor(s). MDPI and/or the editor(s) disclaim responsibility for any injury to people or property resulting from any ideas, methods, instructions or products referred to in the content.